Wavelet Based Damage Detection Approach for Bridge Structures Utilising Vehicle Vibration

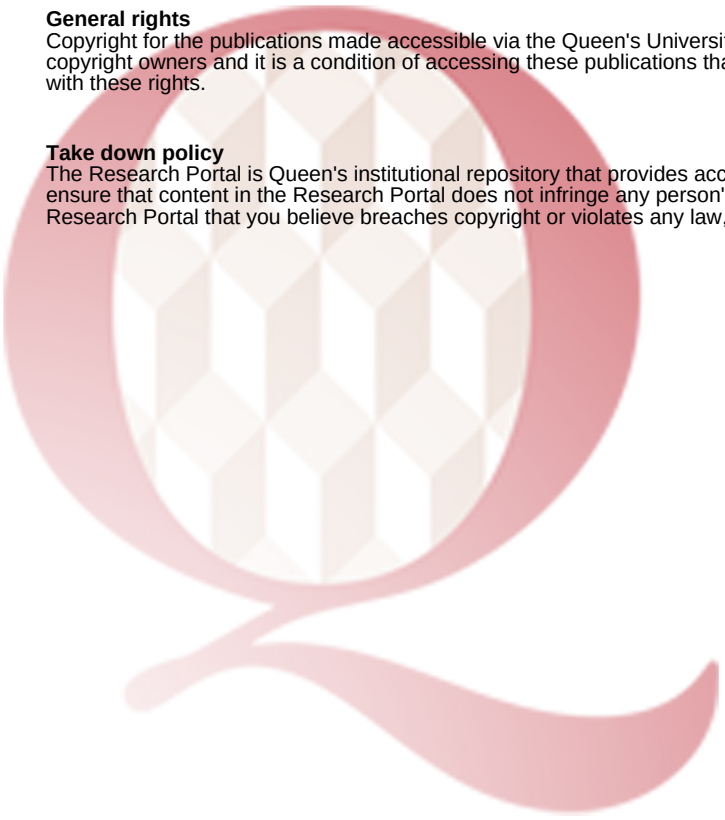

Wavelet Based Damage Detection Approach for Bridge Structures Utilising Vehicle Vibration

Patrick J. McGetrick[1] and Chul Woo Kim[2]

[1] Kyoto University, Kyoto, Japan, mcgetrick.patrickjohn.5x@kyoto-u.ac.jp
[2] Kyoto University, Kyoto, Japan, kim.chulwoo.5u@kyoto-u.ac.jp

Abstract
This paper investigates a wavelet-based damage detection approach for bridge structures. By analysing the continuous wavelet transform of the vehicle response, the approach aims to identify changes in the bridge response which may indicate the existence of damage. A numerical vehicle-bridge interaction model is used in simulations as part of a sensitivity study. Furthermore, a laboratory experiment is carried out to investigate the effects of varying vehicle configuration, speed and bridge damping on the ability of the vehicle to detect changes in the bridge response. The accelerations of the vehicle and bridge are processed using a continuous wavelet transform, allowing time-frequency analysis to be carried out on the responses of the laboratory vehicle-bridge interaction system. Results indicate the most favourable conditions for successful implementation of the approach.
Keywords: acceleration, damage detection, damping, vehicle-bridge interaction, wavelet transform

1. INTRODUCTION

Over the past two decades there has been a focus on the development of effective techniques for the monitoring of the condition of structures such as bridges. These structural health monitoring (SHM) techniques [1-3], the majority of which are vibration based, generally require measurement gauges and data acquisition electronics to be installed directly on the bridge, which can be difficult and time consuming. However, they can be effective in providing a warning to public if a bridge's condition deteriorates and it becomes unsafe. Due to the ageing of existing bridge stocks worldwide, these approaches are arguably becoming a more critical part of bridge management systems and maintenance strategies. More recently, there has been a move towards the development of indirect vibration-based approaches utilising the response of a vehicle passing over a bridge. This type of approach aims to reduce or eliminate the need for direct instrumentation of the bridge thus providing a more efficient and low-cost alternative.

This paper investigates such an approach; an alternative wavelet-based approach for the periodic monitoring of bridge structures which consists of the use of a vehicle fitted with accelerometers on its axles. The aim of the approach is to utilise the vehicle response to detect changes in the bridge response which correspond to variations in the structural condition, i.e., damage. In this paper, the effectiveness of this approach is investigated both theoretically and experimentally.

To date, the use of this type of indirect approach to identify bridge properties has been investigated by many researchers. The feasibility of extracting the natural frequency of a bridge from the acceleration response of a passing vehicle has been verified theoretically [4-7]. Yang et al. [4] use a tractor-trailer system in simulations; the tractor serves as the exciter of the bridge while the trailer acts as the receiver of the bridge vibration. The bridge frequency is extracted from the spectra of the vehicle accelerations. In addition, they find that the magnitude of the peak response in the vehicle acceleration spectra increases with vehicle speed but decreases with increasing bridge damping ratio. McGetrick et al. [6] identify both the frequency and changes in damping of the bridge from vehicle accelerations and note that it is difficult to detect both of these parameters in the presence of a rough road profile. Yang et al. [4] and González et al. [7] both highlight that frequency matching between the vehicle and the bridge is beneficial for frequency detection. Yang and Chang [8] present a parametric study which indicates some of the best conditions for frequency detection using this type of indirect approach.

Field trials have taken place to investigate a drive-by inspection method for bridges [9-12]. It is found that accurate determination of the bridge natural frequency is feasible for low speeds and when there is sufficiently high dynamic excitation of the bridge. This is due to the road roughness having a greater influence than bridge vibration on the vehicle response. The empirical mode decomposition technique is used by Yang and Chang [12] to extract frequencies of higher modes from the vehicle response. Experimental investigations have also been conducted to examine the feasibility of such an approach as part of a drive-by inspection system for bridge monitoring. In a laboratory experiment, Toshinami et al. [13] extract the bridge frequency from the dynamic response of a vehicle. Kim and Kawatani [14] investigate a condition screening and damage detection approach which utilises an inspection car, acting as an actuator to the bridge, for data acquisition from wireless sensor nodes installed on the bridge. It is found that the damage location and severity is identified by the approach via analysis and comparison of the stiffness distribution throughout the bridge between intact and damaged states.

Bu et al. [15] also present a numerical investigation of a bridge condition assessment technique which utilises the dynamic response of a vehicle moving along a beam to detect damage in terms of stiffness reduction. They find that vehicle speed, measurement noise, road surface roughness and model errors do not have a significant effect on the accuracy of the approach. González et al. [16] also present a novel algorithm which, using the vehicle accelerations as the

input, identifies the damping of a bridge. It is found that the algorithm can also be used to identify the bridge stiffness and is not very sensitive to low levels of signal noise, the road roughness or errors in the assumed numerical models.

The popularity of wavelet theory and in particular, the use of wavelets in techniques to identify structural damage, has risen considerably in recent years as it allows a signal to be analysed in both time and frequency domains simultaneously. Hester and González [17] provide examples demonstrating the capacity of the wavelet transform to capture time-frequency information while Reda Taha et al. [18] discuss the use of wavelet analysis in structural health monitoring applications. Their use has also been extended to indirect approaches for the purpose of damage detection.

Nguyen and Tran [19] present a wavelet based approach to identify cracks in a bridge from the vehicle response. Numerical simulations are carried out using a cracked finite element (FE) beam model and a 4 degree-of-freedom half-car vehicle model however no road profile is included. The aim is to determine the existence and location of cracks in the beam from the vehicle displacement response using the Symlet wavelet transform. A two-crack scenario is investigated varying vehicle speed and crack depth is also varied as a percentage of the beam depth. Peaks at particular scales are observed in the wavelet transform of the vehicle displacement response when it passes over cracks while crack depths of up to 10% are detected. It is found that deeper cracks are easier to detect while higher speeds provide poorer detection ability. The effect of white noise on crack detection is investigated and for 6% noise, a 50% crack depth is detected at 2 m/s. Experimental testing is recommended by the authors.

Khorram et al. [20] also carry out a numerical investigation in which a very simple vehicle-bridge interaction (VBI) model is used to compare two methods which utilise a wavelet transform to identify the existence and location of cracks in beams; a "fixed sensor approach" and a "moving sensor approach", which are direct and indirect methods respectively. Using the Gaussian 4 mother wavelet, the continuous wavelet transforms (CWTs) of beam and vehicle displacements are used to identify cracks which are modelled as rotational springs connecting elements. The moving sensor is found to be more effective than the fixed sensor and small cracks with a depth of more than 10% of beam depth are detected. The authors develop a damage index which has an explicit expression and can identify crack depth as well as location.

In this paper, the aim is to investigate the effectiveness of wavelet based indirect approach for the monitoring of bridges which uses vehicle accelerations. Firstly, in theoretical simulations, a simplified VBI simulation model is created in MATLAB [21] and is used to investigate the effectiveness of the approach in detecting damage in a bridge. A time-frequency analysis is carried out in order to identify the existence and/or location of two types of damage from the vehicle accelerations. For this purpose, the accelerations are processed using a CWT. Bridge span length, vehicle speed, road roughness and damage severity and/or location are varied in simulations to investigate the effect on the accuracy of results. Secondly, in the laboratory, a scaled vehicle-bridge model is used which consists of a scaled two-axle vehicle and a simply supported steel beam, which incorporates a scaled road surface profile. This experiment is carried out to validate results of the theoretical analysis and investigate the effects of varying vehicle configuration and speed on the ability of the approach to detect changes in the bridge response from the CWT of vehicle accelerations.

2. METHODOLOGY

2.1. Vehicle-Bridge Interaction Model

The VBI model used in theoretical simulations is a coupled system (Fig. 1) with the solution given at each time step using the Wilson-Theta direct integration scheme. Similar models incorporating the coupling of the vehicle and bridge can be found in the literature [22, 23] and González [24] has carried out reviews of these and other models.

The vehicle model is represented by a 2 degree of freedom half-car which crosses the bridge model at constant speed c (Fig. 1). The two degrees of freedom of the model correspond to sprung mass bounce displacement, y_s, and sprung mass pitch rotation, θ_s. The vehicle body and axle component masses are represented by the sprung mass, m_s = 18000 kg. A combination of springs of linear stiffness K_i = 1.42 × 10^6 N/m and viscous dampers with damping coefficient C_i = 10 × 10^3 N s/m represent the suspension components for the front and rear axles (i = 1, 2). Also, I_s = 103840 kg m^2 is the sprung mass moment of inertia and the distance of each axle to the vehicle's centre of gravity (o) is given by D_i = 2.375 m. (i = 1,2). The vehicle has both bounce and pitch frequencies of 2 Hz. The equations of motion of the vehicle are obtained by imposing equilibrium of all forces and moments acting on the vehicle and expressing them in terms of the degrees of freedom. Then, the vehicle system can be written for the purpose of coupling with the bridge model as:

$$\mathbf{M_v}\ddot{\mathbf{y}}_\mathbf{v} + \mathbf{C_v}\dot{\mathbf{y}}_\mathbf{v} + \mathbf{K_v}\mathbf{y_v} = \mathbf{f_v} \tag{1}$$

where $\mathbf{M_v}$, $\mathbf{C_v}$, and $\mathbf{K_v}$ are, respectively, the mass, damping and stiffness matrices of the vehicle while $\mathbf{f_v}$ is the time varying force vector applied to the vehicle and $\mathbf{y_v} = \{y_s, \theta_s\}^T$ is its displacement vector. Sprung mass acceleration measurements are recorded above the suspension of each axle in simulations (Fig. 1) and the relationship between the degrees of freedom of the vehicle and the measurements is defined by the following equation:

$$\ddot{y}_{s,i} = \ddot{y}_s - (-1)^i D_i \ddot{\theta}_s \; ; \; i = 1,2 \tag{2}$$

The bridge is represented by a simply supported FE beam model (Fig. 1) of total span length L. It consists of discretised beam elements with 4 degrees of freedom which have constant mass per unit length, μ, modulus of elasticity E and second moment of area J. It follows that the beam element stiffness is the product of E and J, denoted EJ. The response of the beam model to a series of moving time-varying forces is given by the system of equations:

$$\mathbf{M_b}\ddot{\mathbf{w}}_\mathbf{b} + \mathbf{C_b}\dot{\mathbf{w}}_\mathbf{b} + \mathbf{K_b}\mathbf{w_b} = \mathbf{N_b}\,\mathbf{f_{int}} \tag{3}$$

where $\mathbf{M_b}$, $\mathbf{C_b}$ and $\mathbf{K_b}$ are ($n \times n$) global mass, damping and stiffness matrices of the beam model respectively, $\mathbf{w_b}$, $\dot{\mathbf{w}}_\mathbf{b}$ and $\ddot{\mathbf{w}}_\mathbf{b}$ are the ($n \times 1$) global vectors of nodal bridge displacements and rotations, their velocities and accelerations respectively, and $\mathbf{N_b f_{int}}$ is the ($n \times 1$) global vector of forces applied to the bridge nodes. The location matrix $\mathbf{N_b}$ consists of zero entries and Hermitian shape function vectors, N_i. The parameter, n is the total number of degrees of freedom of the bridge. Rayleigh damping is adopted here to model the damping of the experimental beam:

$$\mathbf{C_b} = \alpha\,\mathbf{M_b} + \beta\,\mathbf{K_b} \tag{4}$$

where α and β are constants. The damping ratio ξ is assumed to be the same for the first two modes and α and β are obtained from $\alpha = 2\,\xi\,\omega_1\,\omega_2/(\omega_1+\omega_2)$ and $\beta = 2\,\xi/(\omega_1+\omega_2)$ where ω_1 and ω_2 are the first two natural frequencies of the bridge [25]. The properties of the three bridge spans used in simulations are given in Table 1.

The vehicle and bridge systems are coupled at the contact point of the wheel via the interaction force $\mathbf{f_{int}}$. Eqs. (1) and (3) are combined to form the coupled system of equations as:

$$\mathbf{M_g}\ddot{\mathbf{u}} + \mathbf{C_g}\dot{\mathbf{u}} + \mathbf{K_g}\mathbf{u} = \mathbf{f} \tag{5}$$

where $\mathbf{M_g}$ is the combined system mass matrix, $\mathbf{C_g}$ and $\mathbf{K_g}$ are coupled time-varying system damping and stiffness matrices respectively and $\mathbf{f}$ is the system force vector (see Appendix A). Also, $\mathbf{u} = \{\mathbf{y_v}, \mathbf{w_b}\}^\mathbf{T}$ is the displacement vector of the system. Eq. (5) is solved using the Wilson-Theta integration scheme [26, 27] using the optimal value of the parameter $\theta = 1.421$ for unconditional stability [28].

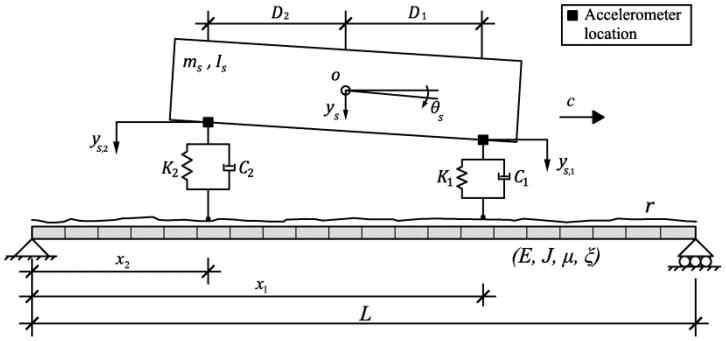

Fig. 1 Vehicle-Bridge Interaction Model

Table 1 Finite element beam properties

Span Length, L (m)	Intact Element Stiffness, EJ (N m^2)	Mass per unit length, μ (kg/m)	Damping, ξ (%)	1st natural frequency of vibration, $f_{b,1}$(Hz)
15	1.846×10^{10}	28 125	3	5.66
25	4.865×10^{10}	18 358	3	4.09
35	1.196×10^{11}	21 752	3	3.01

2.2. Experimental Setup

The experimental setup is shown in Fig. 2(a). A scaled two–axle vehicle model (Fig. 2(b)) is fitted with 2 accelerometers to monitor the vehicle bounce motion; these are located at the centre of the front and rear axles respectively. It also includes a wireless router and data logger which allow the acceleration data to be recorded remotely. The vehicle model can be adjusted to obtain different axle configurations and dynamic properties. The properties of the three vehicle model configurations chosen for these experiments are given in Table 2. The axle spacing and track width for all models were 0.4 m and 0.2 m respectively. The speed of the vehicle was maintained constant by an electronic controller as it crossed the bridge while its entry and exit to the beam was monitored using strain sensors. The scaled vehicle speeds adopted for the experiment are S1 = 0.93 m/s and S2 = 1.63 m/s.

The scaled bridge model used in the experiment simply supported steel beam with span, L_{exp}, of 5.4 m (Fig. 2(c)) which incorporates a scaled road surface profile. It is fitted with accelerometers and displacement transducers at quarter span, mid-span and three-quarter span to measure its response during vehicle crossings. For the experiment, three damping scenarios are investigated, named Intact, C and ABCDE. The Intact scenario represents the beam with no adjustments. Scenarios C and ABCDE represent the beam with its damping adjusted; old displacement transducers are applied at particular points on the beam in addition to a 17.8 kg mass added at midspan. The layout of these "dampers" is illustrated in Fig. 2(a). The old transducers provide frictional resistance to bridge displacements at the chosen locations and hence increase the damping. The additional mass adjusts the frequency of the beam as often damage which causes changes in damping may cause some changes in frequency also. The beam properties are given in Table 3. A sampling frequency of 100 Hz is used in the experiments.

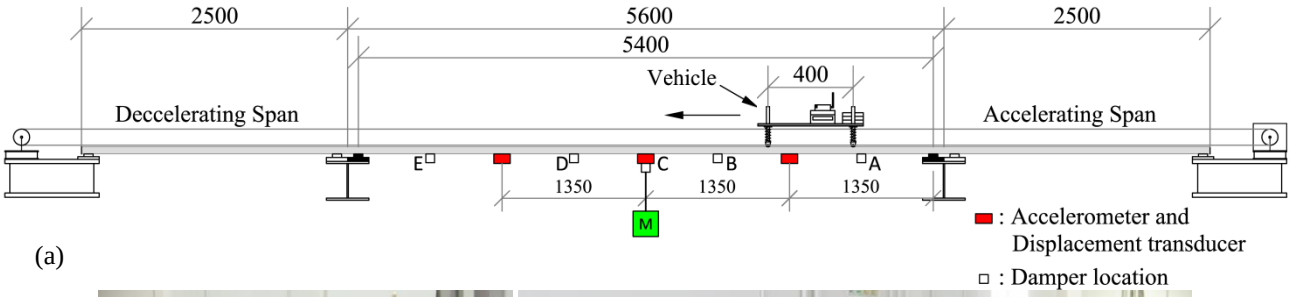

(a)

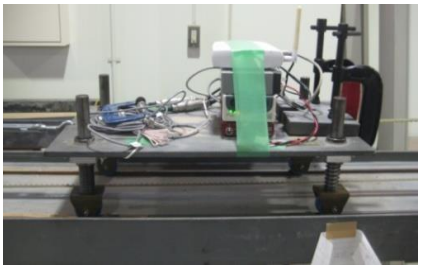

(b)

(c)

Fig. 2 (a) Elevation of laboratory setup (b) Experimental Vehicle (c) Experimental Beam

Table 2 Experimental vehicle model properties

Vehicle	Mass (kg)		Suspension stiffness (N/m)		Suspension damping (N s/m)		Frequency (Hz)	
	Axle 1	Axle 2	Axle 1	Axle 2	Axle 1	Axle 2	Bounce	Pitch
V1	7.9	13.445	2680	4570	16.006	27.762	2.93	4.24
V2	7.9	13.445	4290	7310	13.991	35.112	3.62	5.35
V3	8.355	17.530	2700	5940	18.023	65.829	2.91	3.62

Table 3 Experimental beam model properties

Scenario	Material density, w (kg/m^3)	Cross sectional area, A (m^2)	Stiffness, EJ_{exp} (N m^2)	First natural frequency, $f_{b,exp}$f$_{b,1}$ (Hz)	Damping Ratio, ξ_{exp}
Intact	7800	6.7×10^{-3}	115,400	2.69	0.016
C				2.54	0.027
ABCDE				2.54	0.064

2.3. Continuous Wavelet Transform

The continuous wavelet transform (CWT) of a function $f(t) \in L^2(\mathbf{R})$ is given as [29]:

$$Wf(a,b) = \int_{-\infty}^{\infty} f(t) \frac{1}{\sqrt{a}} \psi^* \left(\frac{t-b}{a} \right) dt \tag{6}$$

where * indicates the complex conjugate of the mother wavelet function, $\psi(t) \in L^2(\mathbf{R})$, shown in Eq.(7):

$$\psi_{a,b}(t) = \frac{1}{\sqrt{a}} \psi \left(\frac{t-b}{a} \right) \tag{7}$$

The wavelet function is scaled by a and translated by b. The mother wavelet adopted for this investigation is the Morlet wavelet, described by Eq.(8). It is a real valued symmetrical wavelet and is selected for this analysis based on a preliminary study of the performance of a number of mother wavelets including Mexican Hat and Gaussian. Time localisation is an important criterion for this approach in order to detect the damage location and it is found that the Morlet wavelet provides the best balance between time and frequency resolution for the approach presented in this paper.

$$\psi(t) = e^{-\frac{t^2}{2}}\cos(5t) \tag{8}$$

This CWT is applied to both the bridge and vehicle acceleration responses obtained in theoretical simulations and the experiment and they can then be analysed in both time and frequency domains simultaneously for the purpose of damage detection. This also enables comparison between the wavelet coefficients of healthy and damaged cases. It should be noted that all acceleration signals are normalized using their standard deviations before applying the CWT.

3. THEORETICAL SIMULATIONS

The aim of the theoretical simulations is to carry out a parametric study of the wavelet based indirect approach effectiveness in detecting changes in the bridge response which may indicate the existence of damage. For this purpose, two different types of damage are considered. The first type of damage (Type 1) is applied via beam element stiffness reduction, corresponding to localized damage within the bridge. The second type (Type 2) is applied via beam damping variation corresponding to a global effect of damage within the bridge. Damping has not been the focus of many damage detection techniques due to difficulties in quantifying its magnitude but recently it has been shown that it can be quite sensitive to damage in structural elements [30-32]. In simulations for both damage types, bridge span lengths of 15 m, 25 m and 35 m, vehicle speeds of 2, 5, 10 and 20 m/s and smooth and rough road profiles are tested. In addition, the severity and location of the damage are varied for Type 1; 0% (healthy), 10% and 40% (damaged) stiffness reductions are investigated which are applied separately to a beam element at either $L/2$ or $5L/8$. Finally, for Type 2, the beam damping level is varied from 1% to 5% (in steps of 1%) in simulations to investigate the sensitivity of the approach in detecting those changes. A sampling frequency of 100 Hz is used in all simulations.

3.1. Damage Type 1: element stiffness reduction

The effect of bridge span length

Fig. 3 shows examples of the difference between wavelet coefficients of axle accelerations obtained for the healthy and 10% damage scenarios for all bridge spans tested. The vehicle speed is 2 m/s while 10% damage is considered at $L/2$. Here, the damage is detected at the vehicle frequency response of 2 Hz, marked at the white lines representing entry and exit of the axle on the damaged beam element. It can be seen that the overall maximum amplitude increases as the span length increases and the time localisation improves also. However, as the bridge span increases, the bridge frequency becomes closer to the vehicle frequency, reducing the dominance of the damage peaks detected by the vehicle. This indicates it may be beneficial to select a vehicle with frequencies which are not close to the bridge frequency.

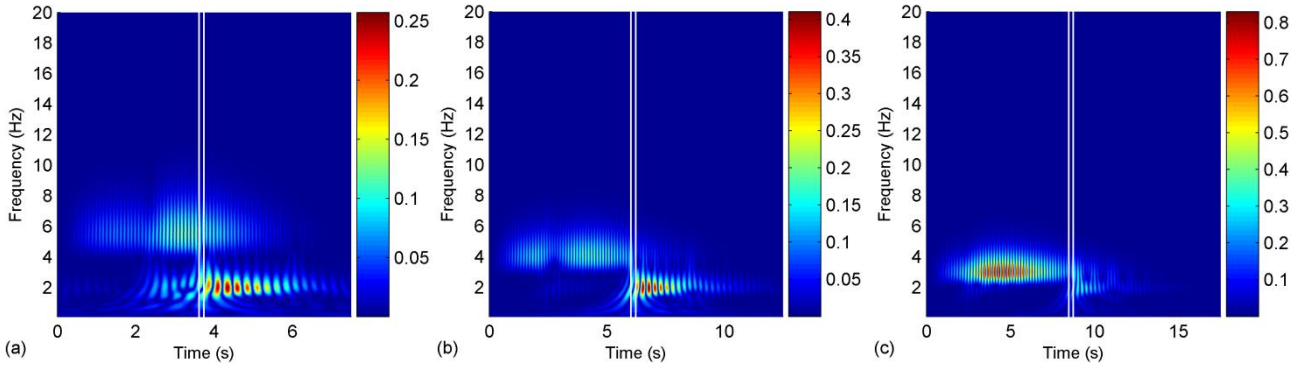

Fig. 3 Difference between wavelet coefficients of axle 1 accelerations on (a) 15 m span (b) 25 m span (c) 35 m span; speed is 2 m/s, damping is 3%, damage severity 10%, smooth road profile.

The effect of vehicle speed

Fig. 4 shows examples of the difference between wavelet coefficients of axle accelerations obtained for the healthy and 10% damage scenarios on the 15 m bridge span for all speeds tested. The corresponding results for 2 m/s are omitted here as they are shown in Fig. 3(a). It can be seen that as the speed increases, it becomes more difficult to accurately identify the existence and location of the damage. This is primarily due to the reduction in resolution that occurs for higher speeds due to the response time history becoming shorter. This suggests lower vehicle speeds are best for use with this approach.

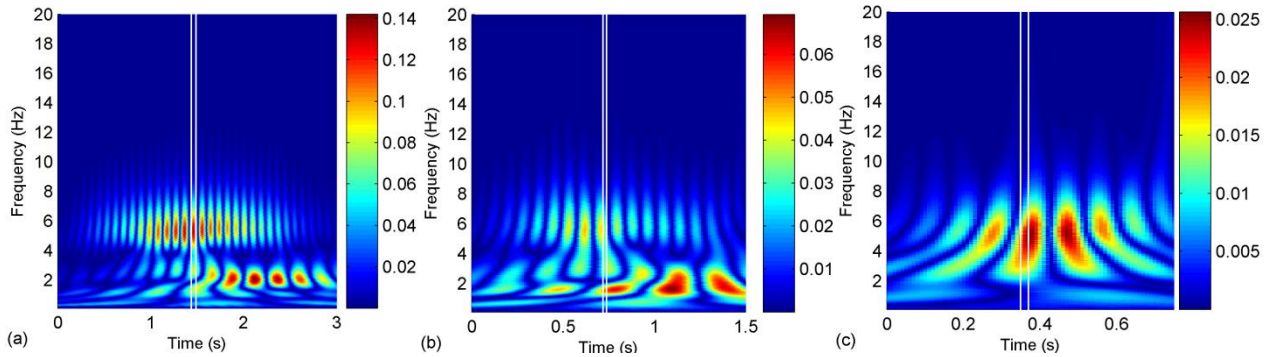

Fig. 4 Difference between wavelet coefficients of axle 1 accelerations for 15 m span (a) 5 m/s (b) 10 m/s (c) 20m/s; damping is 3%, damage severity 10%, smooth road profile.

The effect of damage severity and location

Fig. 5(a) illustrates the difference between wavelet coefficients of axle accelerations obtained for the healthy and 40% damage scenarios on the 15 m bridge span for 2 m/s. Comparing Fig. 3(a) and Fig. 5(a), the effect of increasing the damage severity at $L/2$ can be observed. For increased damage severity, it is found that the only significant change is in the overall coefficient peak amplitudes, which increase. This indicates that the peak magnitude may be utilized for quantification of damage severity.

Fig. 5(b) shows the wavelet coefficients corresponding to the scenario represented in Fig. 5(a), except now considering a different damaged element location at $5L/8$. Comparing Fig. 5(b) and Fig. 5(a), the overall coefficient magnitude increases and the accuracy of the detection of the damage and its location improves slightly, indicating that this approach can identify the damage location regardless of its position along the bridge span. Here, the increase in accuracy and magnitude can be attributed to the damage location not coinciding with the maximum bridge response, which reduces the dominance of the damage peaks in Fig. 5(a). Similar results are obtained for 10% damage severity at $5L/8$.

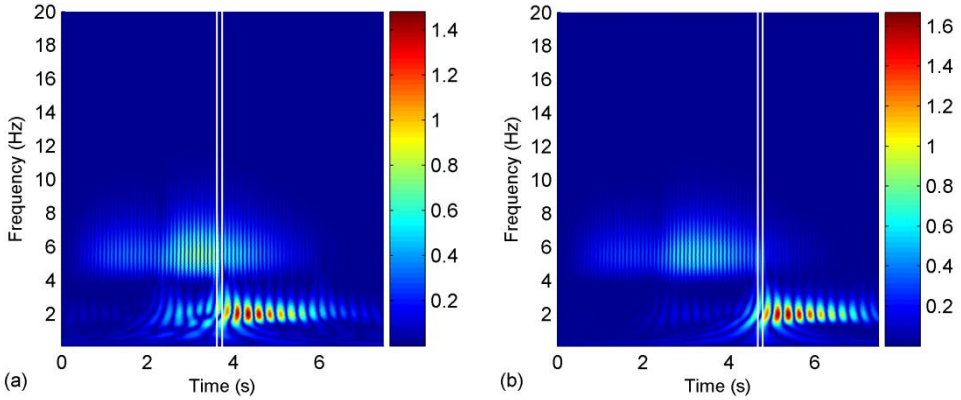

Fig. 5 Difference between wavelet coefficients of axle 1 accelerations for 15 m span (a) damage severity 40% at $L/2$ (b) damage severity 40% at $5L/8$; speed is 2m/s, damping is 3%, smooth road profile.

The effect of road roughness

Results presented thus far were for a smooth road profile. However, as past studies encountered difficulties in detecting changes in the bridge response from the vehicle response in the presence of a rough road profile, this section tests the sensitivity of the approach to the road profile roughness by including an ISO class 'A' (very good) road profile [33] in the simulations. Results corresponding to the 15 m bridge span and a speed of 2 m/s are presented here. Fig. 6(a) shows the wavelet coefficient difference between the healthy and 10% damage scenarios for the very good profile; the damage location is $L/2$. It can be seen that the vehicle vibration dominates in the region of 2 Hz. The dominance of the vehicle response throughout the time history is due to the road profile excitation and although the damage appears to be detected, compared to Fig. 3(a) and Fig. 5(a) it is difficult to accurately confirm its location.

Fig. 6(b) shows the corresponding result for the very good profile using the vehicle model with its spring stiffness increased to 1.42×10^8 N/m to give an axle bounce frequency of 20 Hz. The damage can be detected clearly at a local maximum in the vehicle response for axle 1. This highlights the benefit of a vehicle with frequencies far from the bridge frequency.

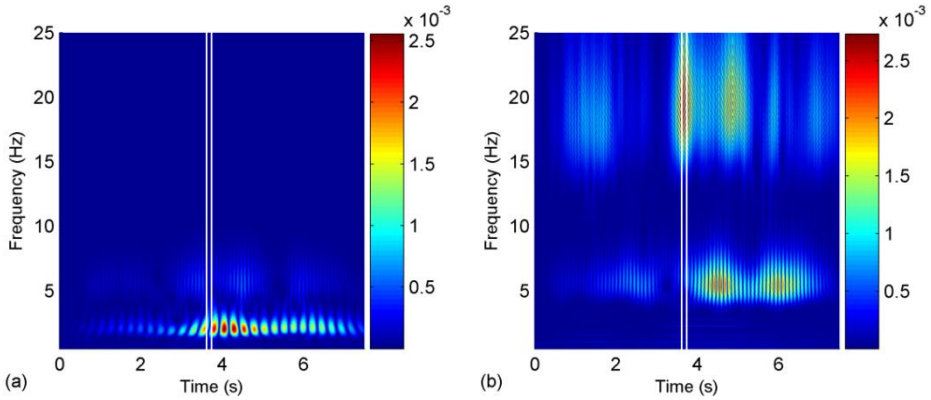

Fig. 6 Difference between wavelet coefficients of axle 1 accelerations for 15 m span with 10% damage at *L*/2 (a) 2 Hz vehicle (b) 20 Hz vehicle; damping is 3%, Class A road profile.

3.2. Damage Type 2: damping variation

The effect of bridge span length

Fig. 7 shows examples of the difference between wavelet coefficients of accelerations obtained for 3% and 5% bridge damping for all spans tested. It can be seen in Fig. 7(a)-(c) that for the damping increase from 3% to 5%, the bridge coefficient amplitude increases with increasing bridge span. The coefficients corresponding to the vehicle are dominated by the bridge frequency and detect this change in the bridge response with damping (Fig. 7(d)-(f)). The vehicle response amplitude increases as the span length increases also, indicating that damping variations may be easier to detect in longer span bridges.

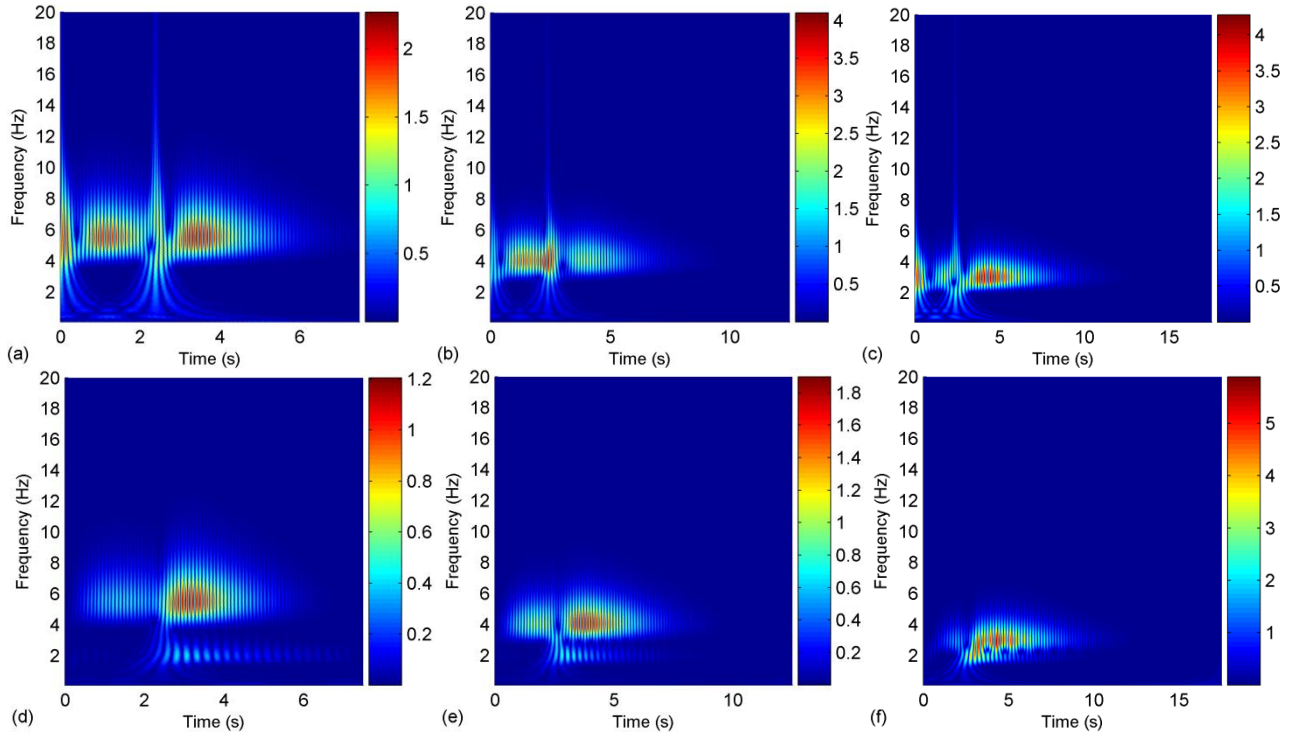

Fig. 7 Difference between wavelet coefficients of accelerations for damping increase from 3% to 5%. Beam midspan for (a) 15 m span (b) 25 m span (c) 35 m span; Axle 1 for (d) 15 m span (e) 25 m span (f) 35 m span; speed is 2 m/s, smooth road profile.

The effect of vehicle speed

The effect of vehicle speed on the ability of this approach to detect the change in damping from 3% to 5% can be examined by studying Fig. 8 for the 15 m bridge span with vehicle speeds of 5 m/s, 10 m/s and 20 m/s. Also comparing Fig. 7(d), it can be seen that the vehicle coefficients are dominated by the bridge frequency and decrease with increasing speed. This indicates that the approach has greater sensitivity to changes in damping at lower vehicle speeds.

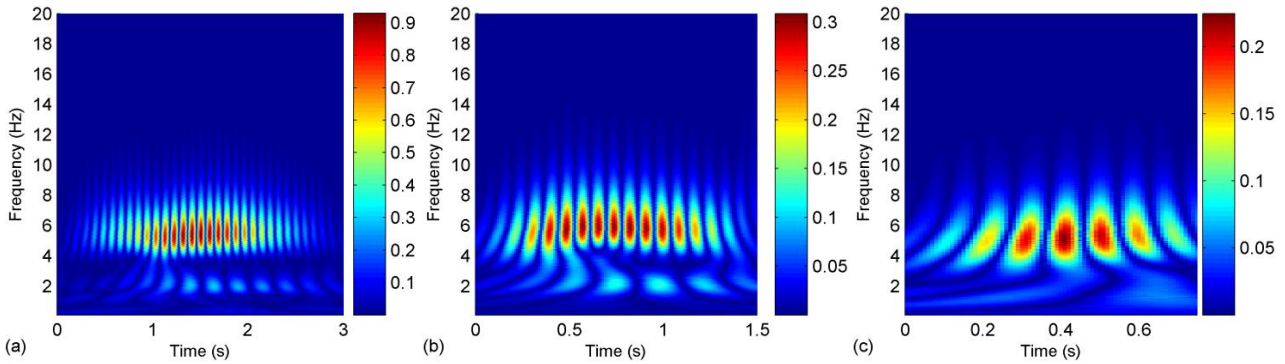

Fig. 8 Difference between wavelet coefficients of axle 1 accelerations for damping increase from 3% to 5% in 15 m span. (a) 5 m/s (b) 10 m/s (c) 20 m/s; smooth road profile.

The effect of damping level

Fig. 9(a) and (b) show wavelet coefficients corresponding to Fig. 7(a) and (d) respectively. However, in Fig. 9 results are shown for a smaller damping increase of 3% to 4%. Comparing the figures, it can be seen that the coefficient magnitudes in Fig. 9 are smaller for both the bridge and vehicle accelerations, indicating that the magnitude may be used to indicate the size of the damping variation.

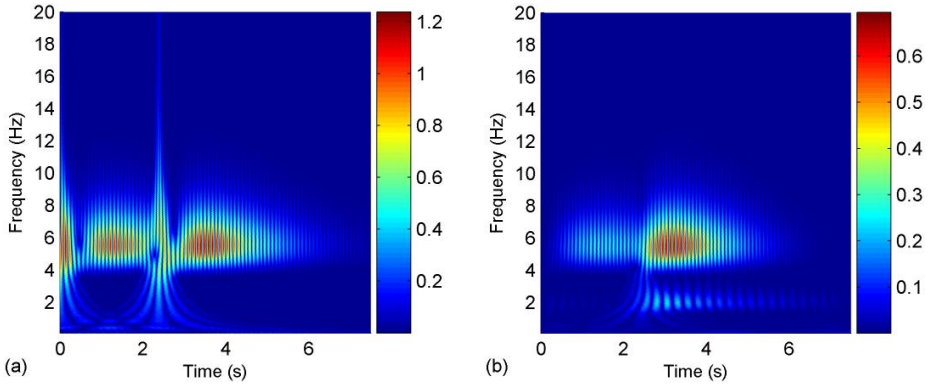

Fig. 9 Difference between wavelet coefficients of accelerations for damping increase from 3% to 4% in 15 m span. (a) Beam midspan (b) Axle 1; speed is 2 m/s, smooth road profile.

The effect of road roughness

To analyse the effect of road profile roughness on the approach, an ISO Class A road profile is included in simulations for the Type 2 damage. Fig. 10 shows an example of the difference between wavelet coefficients of accelerations for a damping increase of 3% to 5% with the Class A profile. The bridge span is 15 m and the vehicle speed is 2 m/s. Fig. 10 can be compared with smooth road profile results shown in Fig. 7(a) and (d). The overall bridge coefficient magnitude does not change significantly but the pattern of the response changes due to the inclusion of the Class A road profile. Fig. 10(b) shows that the damping change is detected by the vehicle at both the bridge and vehicle frequencies. However, compared to Fig. 7(d), the magnitude has decreased significantly which shows that the sensitivity of the approach to damping is significantly affected by the road roughness.

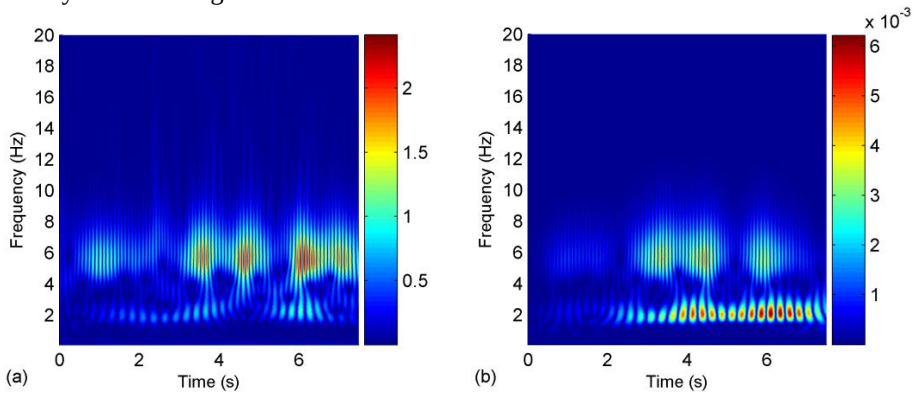

Fig. 10 Difference between wavelet coefficients of accelerations for for damping increase from 3% to 5% in 15 m span. (a) Beam midspan (b) Axle 1; Class A road profile.

4. EXPERIMENTAL INVESTIGATION

This section presents results of the application of the approach to an experiment, based on Type 2 damage. Fig. 11 shows an example of beam and vehicle axle accelerations obtained during the crossing of V1 at S1 for the three damping scenarios investigated. Apart from some spurious peaks in the vehicle accelerations, it can be seen that in general the Intact case provides the largest response. Only results for vehicle V1 are presented here as results for other vehicle models exhibited similar trends.

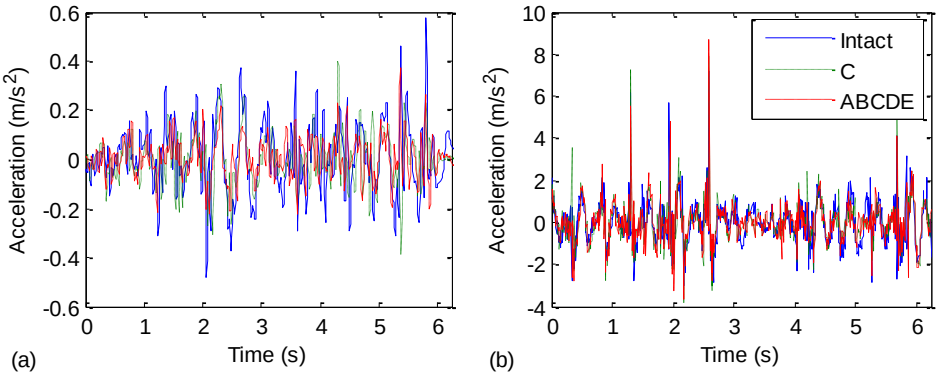

Fig. 11 Vehicle V1 and speed S1; Acceleration responses from three damping scenarios for (a) beam midspan and (b) vehicle axle 1

Fig. 12 shows the absolute wavelet coefficient values from the three damping scenarios investigated for the beam and vehicle V1 with speed S1. It is clear from the bridge coefficients that as the damping increases, the magnitude of the bridge response at its natural frequency (2.69 Hz and 2.54 Hz in the intact and damped cases respectively) decreases. A similar decrease can be observed at the peaks corresponding to the bridge frequency in the wavelet coefficient plots for axle 1 of the vehicle in Fig. 12(d)-(f). From scenario C to ABCDE in Fig. 12(e)-(f), the decrease is not so clear but the overall coefficient magnitude at the vehicle response also decreases. This indicates that the changes in damping can be identified using this approach.

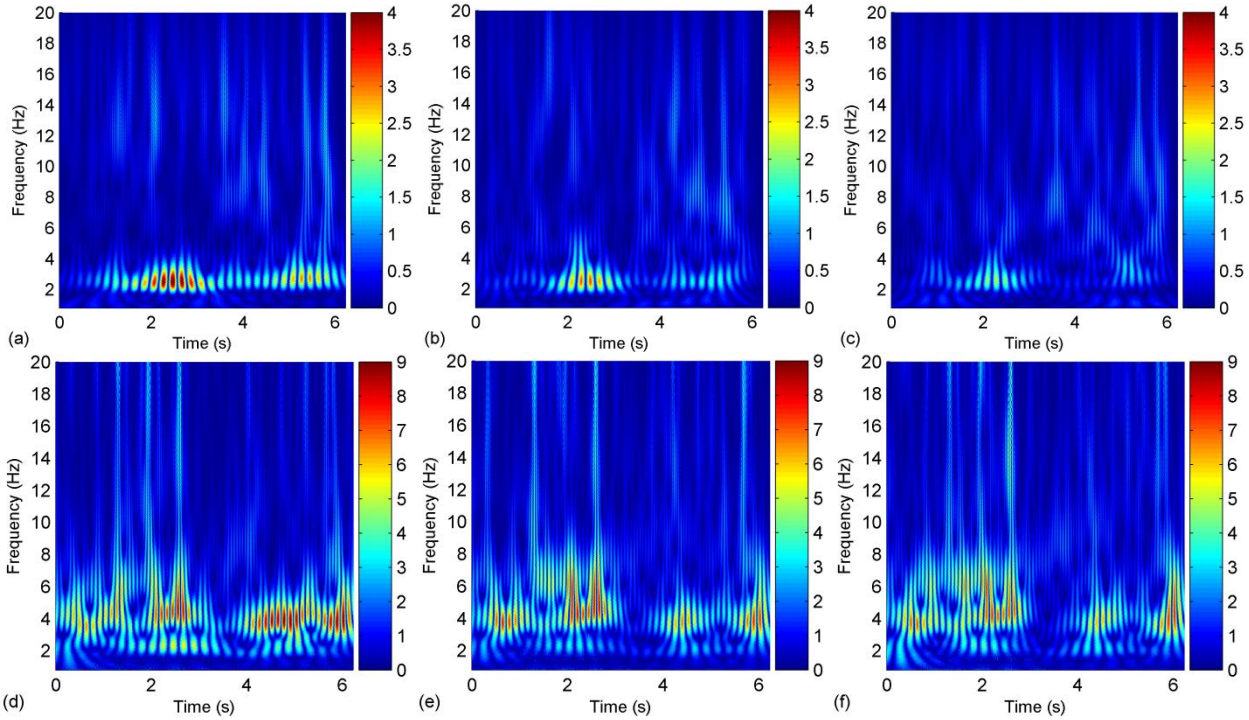

Fig. 12 Wavelet coefficients of accelerations for vehicle V1 and speed S1; for beam midspan (a) Intact (b) C (c) ABCDE; Axle 1 (d) Intact (e) C (f) ABCDE.

As the changes in the vehicle coefficient plots are not so clear in Fig. 12, the difference between the coefficients obtained for the Intact and damped (C and ABCDE) scenarios are calculated to allow for easier observation of the changes with damping. Similar wavelet coefficient difference plots were the focus of the theoretical simulations in the previous section.

Therefore, Fig. 13 shows the difference between wavelet coefficients of accelerations obtained for the beam and axle 1 of the vehicle during the crossing of vehicle V1 at speed S1. The coefficients of C and ABCDE are subtracted from those of the Intact scenario respectively. Fig. 13 shows that the magnitude of the difference increases with increasing damping for both the vehicle and the bridge, matching trends observed in theoretical simulations and suggesting that the overall wavelet spectrum may be used as an indicator of changes in damping. Also, as the vehicle passes the midspan of the bridge, around 3 seconds, a clear change in the magnitude of the bridge frequency response can be found in the vehicle wavelet coefficient plots, matching that of the bridge plots in Fig. 13(a) and (b), hence detecting the changes in damping.

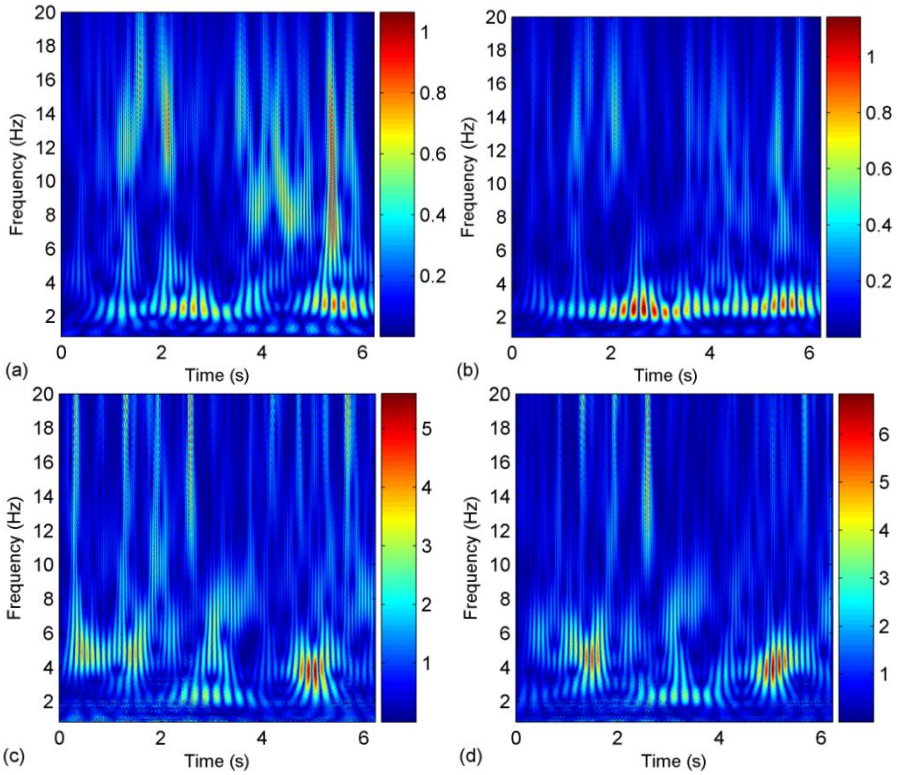

Fig. 13 Difference between wavelet coefficients of accelerations for vehicle V1 and speed S1; beam midspan (a) Intact – C (b) Intact – ABCDE; vehicle axle 1 (c) Intact – C (d) Intact – ABCDE.

Fig. 14 shows the difference between the coefficients obtained for the Intact and damped scenarios for vehicle V1 crossing the beam at speed S2 = 1.63 m/s. Due to the shorter time history, the resolution is reduced and it is difficult to distinguish or detect changes at the bridge frequency. However, the changes in damping are detected primarily at the vehicle pitch frequency of 4.24 Hz and similar to speed S1, the overall magnitude of the coefficient difference increases with increased damping. As similar results were obtained for other vehicle models, this indicates that it is more beneficial to use a lower vehicle speed due to the resolution but higher speed can also provide responses which indicate the changes in damping.

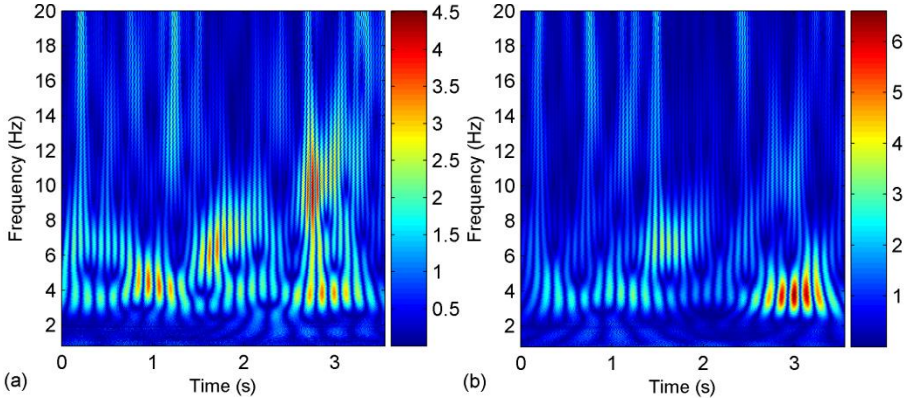

Fig. 14 Difference between wavelet coefficients of accelerations for vehicle V1 and speed S2; vehicle axle 1 (a) Intact – C (b) Intact – ABCDE.

5. CONCLUSIONS

This paper investigates the feasibility of an alternative wavelet-based approach for the periodic monitoring of bridge structures consisting of the use of a vehicle instrumented with accelerometers on its axles. Theoretical investigations are carried out which focus on two types of bridge damage. For damage applied via beam element stiffness reduction, it is found that the approach can detect the existence and location of the damage more accurately for lower vehicle speeds and longer bridge spans due to the time resolution. The damage severity is indicated by the wavelet coefficient magnitude. However, the vehicle frequency should be far from the bridge frequency as the damage is detected in the frequency response of the vehicle. This is found to be beneficial for detecting damage in the presence of a rough road profile.

For damage scenario involving damping changes, it is found that the approach can more accurately detect the changes for longer span bridges and lower vehicle speeds while the coefficient magnitude can also indicate the size of the damping change. Road roughness reduces the sensitivity of the approach to changes in damping considerably.

In an experimental investigation, the results of the theoretical simulations considering changes in bridge damping are validated. It is found that lower vehicle speed is better for this approach due to the time resolution. Overall, this low-cost approach has the potential to be implemented as a tool for the periodic monitoring of bridge condition. Future work will focus on challenges associated with the real world application of this approach and the development of a damage index.

6. ACKNOWLEDGEMENT

The authors wish to express their gratitude for the financial support received from the Japanese Society for the Promotion of Science for the Grant-in-Aid for Scientific Research (B) under project no. 24360178.

7. APPENDIX A

$$\mathbf{M_v} = \begin{bmatrix} m_s & 0 \\ 0 & I_s \end{bmatrix}; \mathbf{C_v} = \begin{bmatrix} C_1 + C_2 & D_1C_1 - D_2C_2 \\ D_1C_1 - D_2C_2 & {D_1}^2C_1 + {D_2}^2C_2 \end{bmatrix}; \mathbf{K_v} = \begin{bmatrix} K_1 + K_2 & D_1K_1 - D_2K_2 \\ D_1K_1 - D_2K_2 & {D_1}^2K_1 + {D_2}^2K_2 \end{bmatrix}$$

$$\mathbf{f_v} = \begin{Bmatrix} \sum_{i=1}^{2} (K_i w_{v,i} + C_i \dot{w}_{v,i}) \\ -\sum_{i=1}^{2} (-1)^i D_i (K_i w_{v,i} + C_i \dot{w}_{v,i}) \end{Bmatrix}$$

$$\mathbf{M_g} = \begin{bmatrix} \mathbf{M_v} & 0 \\ 0 & \mathbf{M_b} \end{bmatrix}; \quad \mathbf{C_g} = \begin{bmatrix} \mathbf{C_v} & \mathbf{C_{vb}} \\ \mathbf{C_{bv}} & \mathbf{C_b} + \mathbf{C_{bb}} \end{bmatrix}; \quad \mathbf{K_g} = \begin{bmatrix} \mathbf{K_v} & \mathbf{K_{vb}} \\ \mathbf{K_{bv}} & \mathbf{K_b} + \mathbf{K_{bb}} \end{bmatrix}$$

$$\mathbf{C_{bv}} = \left[-\mathbf{N_b} \begin{bmatrix} C_1 & D_1C_1 \\ C_2 & -D_2C_2 \end{bmatrix} \right]_{n \times 2}; \ \mathbf{C_{vb}} = \mathbf{C_{bv}}^{\mathbf{T}}; \qquad \mathbf{K_{bv}} = \left[-\mathbf{N_b} \begin{bmatrix} K_1 & D_1K_1 \\ K_2 & -D_2K_2 \end{bmatrix} \right]_{n \times 2}; \ \mathbf{K_{vb}} = \mathbf{K_{bv}}^{\mathbf{T}}$$

$$\mathbf{C_{bb}} = \left[\mathbf{N_b} \left[\mathbf{N_b} \begin{bmatrix} C_1 & 0 \\ 0 & C_2 \end{bmatrix} \right]^T \right]_{n \times n}; \qquad \mathbf{K_{bb}} = \left[\mathbf{N_b} \left[\mathbf{N_b} \begin{bmatrix} K_1 & 0 \\ 0 & K_2 \end{bmatrix} \right]^T \right]_{n \times n}$$

$$\mathbf{f} = \begin{Bmatrix} \sum_{i=1}^{2} (K_i r_i + C_i \dot{r}_i) \\ -\sum_{i=1}^{2} (-1)^i D_i (K_i r_i + C_i \dot{r}_i) \\ \mathbf{N_b} \begin{Bmatrix} P_1 - K_1 r_1 - C_1 \dot{r}_1 \\ P_2 - K_2 r_2 - C_2 \dot{r}_2 \end{Bmatrix} \end{Bmatrix}_{(n+2) \times 1} ; \mathbf{N_b} = \begin{bmatrix} 0 & 0 \\ N_1 & 0 \\ 0 & N_2 \\ 0 & 0 \end{bmatrix}_{n \times 2}$$

8. REFERENCES

[1] Farrar C. and Worden K., "An introduction to structural health monitoring", *Philosophical Transactions of the Royal Society A* 365, pp. 303-315, 2007.

[2] Sohn H., Farrar C.R., Hemez F.M., Shunk D.D., Stinemates D.W. and Nadler B.R., "*A review of structural health monitoring literature: 1996-2001*", Los Alamos National Laboratory Report LA-13976-MS, USA, 2003.

[3] Carden E.P. and Fanning P., "Vibration based condition monitoring: A review", *Structural Health Monitoring* 3(4), pp. 355-377, 2004.

[4] Yang Y.B., Lin C.W. and Yau J.D., "Extracting bridge frequencies from the dynamic response of a passing vehicle", *Journal of Sound and Vibration* 272, pp. 471-493, 2004.

[5] Yang Y.B. and Lin, C.W., "Vehicle-bridge interaction dynamics and potential applications", *Journal of Sound and Vibration* 284, pp. 205-226, 2005.

[6] McGetrick P.J., González A. and OBrien E.J., "Theoretical investigation of the use of a moving vehicle to identify bridge dynamic parameters", *Insight* 51(8), pp. 433-438, 2009.
[7] González A., OBrien E.J. and McGetrick P.J., "Detection of Bridge Dynamic Parameters Using an Instrumented Vehicle", *Proceedings of the Fifth World Conference on Structural Control and Monitoring*, Tokyo, Japan, paper 34, 2010.
[8] Yang Y.B., Chang K.C., "Extracting the bridge frequencies indirectly from a passing vehicle: Parametric study", *Engineering Structures* 31(10), pp. 2448-2459, 2009b.
[9] Lin C.W. and Yang Y.B., "Use of a passing vehicle to scan the fundamental bridge frequencies. An experimental verification", *Engineering Structures* 27: 1865-1878, 2005.
[10] Oshima Y., Yamaguchi T., Kobayashi Y. and Sugiura K., "Eigenfrequency estimation for bridges using the response of a passing vehicle with excitation system", *Proceedings of the Fourth International Conference on Bridge Maintenance, Safety and Management, IABMAS2008*, Seoul, Korea, pp. 3030-3037, 2008.
[11] González A., Covián E. and Madera J., "Determination of Bridge Natural Frequencies Using a Moving Vehicle Instrumented with Accelerometers and GPS", *Proceedings of the Ninth International Conference on Computational Structures Technology*, Athens, Greece, paper 281, 2008.
[12] Yang Y.B., Chang K.C., "Extraction of bridge frequencies from the dynamic response of a passing vehicle enhanced by the EMD technique", *Journal of Sound and Vibration* 322, pp. 718-739, 2009a.
[13] Toshinami T., Kawatani M. and Kim C.W., "Feasibility investigation for identifying bridge's fundamental frequencies from vehicle vibrations", *Proceedings of the Fifth International Conference on Bridge Maintenance, Safety and Management, IABMAS2010*, Philadelphia, USA, pp. 317-22, 2010.
[14] Kim C.W. and Kawatani M., "Challenge for a Drive-by Bridge Inspection", *Proceedings of the 10th International Conference on Structural Safety and Reliability ICOSSAR2009*, Osaka, Japan, pp. 758-765, 2009.
[15] Bu J.Q., Law S.S. and Zhu X.Q., "Innovative bridge condition assessment from dynamic response of a passing vehicle", *Journal of Engineering Mechanics – ASCE* 132(12), pp. 1372-1379, 2006.
[16] González A., OBrien E.J. and McGetrick P.J., "Identification of damping in a bridge using a moving instrumented vehicle", *Journal of Sound and Vibration* 331(18), pp. 4115-4131, 2012.
[17] Hester D. and González A., "A wavelet-based damage detection algorithm based on bridge acceleration response to a vehicle", *Mechanical Systems and Signal Processing*, doi:10.1016/j.ymssp.2011.06.007, 2011.
[18] Reda Taha M.M., Noureldin A., Lucero J.L. and Baca T.J., "Wavelet transform for structural health monitoring: a compendium of uses and features", *Structural Health Monitoring* 5(3): pp. 267–295, 2006.
[19] Nguyen K.V. and Tran H.T., "Multi-cracks detection of a beam-like structure based on the on-vehicle vibration signal and wavelet analysis", *Journal of Sound and Vibration* 329(21), pp. 4455–4465, 2010.
[20] Khorram A., Bakhtiari-Nejad F. and Rezaeian M., "Comparison studies between two wavelet based crack detection methods of a beam subjected to a moving load", *International Journal of Engineering Science* 51, pp. 204–215, 2012.
[21] MATLAB. The MathWorks, Inc., MATLAB, Version 7, USA, 2005. http://www.mathworks.com
[22] Henchi K., Fafard M., Talbot M. and Dhatt G., "An efficient algorithm for dynamic analysis of bridges under moving vehicles using a coupled modal and physical components approach", *Journal of Sound and Vibration* 212(4), pp. 663-683,1998.
[23] Kim C.W. and Kawatani M., "Pseudo-static approach for damage identification of bridges based on coupling vibration with a moving vehicle", *Structure and Infrastructure Engineering* 4(5), pp. 371-379, 2008.
[24] González A., "Vehicle-bridge dynamic interaction using finite element modelling", In: David Moratal, editor. *Finite Element Analysis*. Croatia: Sciyo, pp. 637-662, 2010.
[25] Clough R.W. and Penzien J., "*Dynamics of structures*", McGraw-Hill, 1993.
[26] Bathe K.J. and Wilson EL., "*Numerical methods in finite element analysis*", Prentice Hall, 1976.
[27] Tedesco J.W., McDougal W.G. and Ross C.A., "*Structural Dynamics, Theory and Applications*", Addison-Wesley, 1999.
[28] Weaver W. and Johnston P.R., "*Structural Dynamics by Finite Elem*ents", UK: Prentice-Hall, 1987.
[29] Mallat S., "*A Wavelet Tour of Signal Processing, Third Edition: The Sparse Way*", Academic Press, 3rd edition, 2008.
[30] Curadelli R.O., Riera J.D., Ambrosini D. and Amani M.G., "Damage detection by means of structural damping identification", *Engineering Structures* 30, pp. 3497–3504, 2008.
[31] Modena C., Sonda D. and Zonta D., "Damage localization in a reinforced concrete structures by using damping measurements", *Key Engineering Materials* 167–168, pp. 132–141, 1999.
[32] Gutenbrunner G., Savov, K. and Wenzel H., "Sensitivity studies on damping estimation", *Proceedings of the Second International Conference on Experimental Vibration Analysis for Civil Engineering Structures (EVACES)*, Porto, Portugal, October 2007.
[33] ISO 8608:1995, "*Mechanical Vibration-road Surface Profiles-reporting of Measured Data*", International Standards Organisation (1995).